Clays and Clay Minerals, Vol. 34, No. 4, 359–367, 1986.

THE LORENTZ-POLARIZATION FACTOR AND PREFERRED ORIENTATION IN ORIENTED CLAY AGGREGATES

R. C. REYNOLDS, JR.

Department of Earth Sciences, Dartmouth College
Hanover, New Hampshire 03755

Abstract—A closed-form equation was derived that describes the powder-ring distribution factor as a function of 2θ, soller slit collimation, and σ^*, which is defined as the standard deviation of an axially symmetrical Gaussian orientation function. Methods were developed for measuring σ^* in the reflection mode by means of a $\theta/2\theta$ diffractometer. Six experimental arrangements for a sedimentary chlorite showed widely different intensity ratios of the 001/005 reflections and gave a standard deviation of ±5.8% when corrected by the theory. The absolute integrated intensities of the 003 reflection from eleven illite samples provided an eight-fold maximum range which, when corrected, yielded a standard deviation of ±7.7%.

The intensity distributions within each of two X-ray powder diffraction patterns obtained from instruments with different soller-slit configurations could not be directly compared at low diffraction angles unless corrections, based on σ^*, were introduced to allow for the differences in axial divergence.

Key Words—Chlorite, Illite, Intensity distribution, Lorentz factor, Orientation, Soller slits, X-ray powder diffraction.

INTRODUCTION

The Lorentz-polarization factor is the most important of the experimental quantities that control X-ray intensity with respect to diffraction angle. Its evaluation is essential to any analysis that depends on the intensities of X-ray diffraction maxima. Practical examples of such applications include one-dimensional crystal structure analysis, modeling interstratified clay diffraction patterns, computation of the MacEwan direct-Fourier transform (MacEwan, 1956), and quantitative analysis of clay mixtures.

The Lorentz-polarization factor Ξ, is given by

$$\Xi = \frac{1 + \cos^2 2\theta\psi}{\sin 2\theta}, \qquad (1)$$

where $1 + \cos^2 2\theta$ denotes the polarization factor, $\sin 2\theta$ describes the change in irradiated volume of a crystal as a function of 2θ (the single crystal Lorentz factor), and ψ is the powder ring distribution factor, the quantity that is the subject of this report. ψ is proportional to $1/\sin\theta$ for a random powder, and its value is constant for a single crystal.

The usual procedure is to select either the single crystal or the random powder form of ψ, but as will be shown below, either may be inappropriate at low diffraction angles. The low-angle values for ψ depend strongly on the degree of preferred orientation of the crystallites that make up the sample and on the soller slit divergences of the diffractometer. The elimination of one of the soller slits on some newer instruments means that relative intensities cannot be directly compared between these "newer" and most "older" machines unless provision is made for differences in the effective Lorentz factors.

An analysis of ψ was undertaken earlier (Reynolds, 1976), but that work is unsatisfactory in several respects. Corrections were applied to low-angle Debye-Scherrer arcs that were slit-length limited. Further consideration has convinced the writer that such a procedure is incorrect for clay minerals which characteristically give broad diffraction maxima, though it should be applicable to coarse-grained micas whose diffraction lines are sharp. The correction has been eliminated here. The earlier work required numerical solutions of the requisite integrals, and the computation time required made such a procedure impractical for many applications. The present work shows the derivation of a closed form equation which, though it contains approximations, is accurate to within a few percent. Finally, the earlier work is incomplete because no consideration was given to the axial divergence of the primary incident beam. The importance of this omission was brought home to the writer with the implementation of a new Siemens D-500 diffractometer which employs no primary-beam soller slit. Important differences in relative intensities of low-angle peaks from well-oriented samples were noted between patterns from the D-500 instrument and patterns produced by an older Diano (General Electric) XRD-5 apparatus which utilizes two soller slits.

The discussion here applies only to the $00l$ or basal reflections from a clay aggregate, the crystallites of which have a mean plate orientation that parallels the surface of the specimen. No lineation is assumed, thus the orientation function is symmetrical about an axis that is normal to the sample surface. Such an orientation is produced by any of the standard preparation methods that involve gravity or centrifuge settling methods, or pressure or filtration techniques. The smear method

produces an essentially unknowable orientation function, and the theory discussed here is inapplicable to such preparations.

THEORY

Figure 1 shows two Debye-Scherrer rings, generated by a parallel incident beam impinging upon an increment of powder that is located on a line normal to P = 0. The distribution of diffraction spots within the rings is meant to depict preferred orientation of the type described above. The two vertical lines separated by D represent two plates of a diffracted-beam soller slit assembly. D is a length, and it is related to the angular divergence of the diffracted beam soller slit, s_2, by

$$D = r_0 \tan s_2, \tag{2}$$

where r_0 is the goniometer radius. The usual nomenclature for slits gives the angular divergence as the sum of the values for the plus and minus directions. Here, one-half of such values will be used. The quantity $\Delta 2\theta$ depicts the small angular increment within which diffraction can occur.

A vector between the projection of P = 0 and the powder ring has the length $r_0 \sin 2\theta$ (Reynolds, 1976), and the portion of the ring intercepted by the detector is given by

$$a = \sin^{-1}\left[\frac{r_0 \tan s_2}{r_0 \sin 2\theta}\right] \approx \sin^{-1}\left[\frac{s_2}{\sin 2\theta}\right]. \tag{3}$$

Soller slit divergences are always small (<5°), so angles can be accurately substituted for tangents and sines. The arcsine can also be replaced by its argument for the same reason, although considerably larger errors are involved which are evaluated later and found to be acceptable. Multiplication by $\cos\theta$ is necessary to obtain the number of crystallites oriented in such a way as to diffract into D (Reynolds, 1976); thus,

$$a \approx \frac{s_2 \cos\theta}{\sin 2\theta} = \frac{s_2}{2 \sin\theta}. \tag{4}$$

Suppose that the orientation of crystallites in a powder is such that a Gaussian form describes the frequency of tilt angles about the plane defined by the sample surface. The function is completely described by the standard deviation, σ^*. Let the intensity diffracted into D be ψ, the powder ring distribution factor. ψ is the integral of the orientation function between the limits zero and a, or

$$\psi = \int_{x=0}^{x=a} \exp(-x^2/2(\sigma^*)^2\, dx = \frac{\sqrt{\pi}}{2} \operatorname{erf}(a/\sqrt{2}\sigma^*), \tag{5}$$

where erf is defined by Eq. (11) below.

The intensity intercepted from each ring, ψ, is given by the number of spots that lie within D, according to

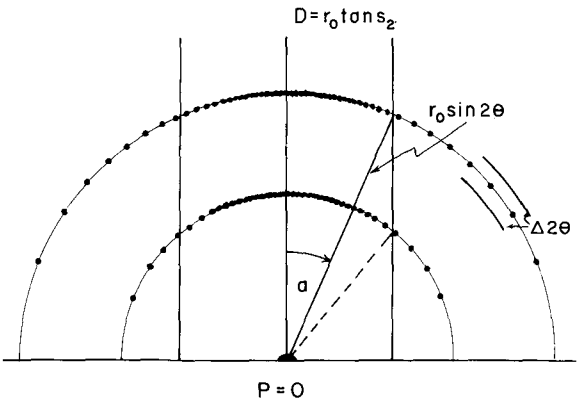

Figure 1. Debye-Scherrer rings from a sample located on a line normal to the figure and intersecting P = 0. Vertical lines are soller slit plates; r_0 is the goniometer radius; s_2 is the angular divergence of the diffracted beam soller slit.

Eq. (5). Suppose that s_2 is small and that θ is large; then a is small (Eq. (4)). If, in addition, σ^* is large,

$$\operatorname{erf}\left(\frac{a}{\sqrt{2}\sigma^*}\right) \propto a \propto \frac{1}{\sin\theta}, \tag{6}$$

and ψ has the random powder form. For opposite conditions, small σ^*, small θ, and large s_2, the value of the error function approaches a constant quantity for the infinite integral, and this defines ψ for the single crystal Lorentz factor. Between these extremes, however, the integral (Eq. (5)) must be solved.

The treatment thus far considers only the diffraction of a parallel incident beam from a small increment of powder. Eq. (5) is the first of three integrations that are required. The other two involve integration over the powder surface and integration over the range of incident angles provided by the primary or incident beam soller slit, s_1.

Figures 2a and 2b are views of the geometry of Figure 1 as seen from above. For a three-dimensional projection of the system, see Reynolds (1976). The axis of the diffracted beam soller slit lies in the horizontal direction, and two plates from this assembly are located by the two heavy horizontal lines. An increment of powder is located at Ps_2 where P is the decimal fraction of the angle s_2. A portion of the incident beam makes the angle A with respect to the axis of the soller slit, and the maximum value of A is equal to s_1, the angular divergence of the incident beam soller slit.

Figures 2a and 2b treat, respectively, the lower limit (x_1) and the upper limit (x_2) of the integral of Eq. (5). The lower limit of integration, x_1, is given by (see Eq. (3) and Eq. (4))

$$x_1 = \cos\theta \sin^{-1}\left[\frac{r_0 \tan A - r_0 P \tan s_2}{r_0 \sin 2\theta}\right] \approx \frac{A - Ps_2}{2 \sin\theta}. \tag{7}$$

Here, $\tan A - r_0 P \tan s_2$ has been substituted for $\tan s_2$ in Eq. (3), and the arcsine has been multiplied by $\cos\theta$ (Eq. (4)). The upper limit of integration (Figure 2b), using similar arguments, is

$$x_2 = \frac{A + (1 - P)s_2}{2 \sin\theta}. \quad (8)$$

The final result requires additional integration of Eq. (5) over the ranges $A = 0$ to $A = s_1$, and $P = 0$ to $P = 1$. In addition, a correction must be applied to account for the flux of X-radiation transmitted by the incident beam soller slit at an angle A. A and s_1 are small, so no appreciable error is involved in substituting arguments for tangents, and the correction is simply

$$1 - \frac{A}{s_1}. \quad (9)$$

The final form for ψ, then, is

$$\psi = \frac{1}{\sigma^*} \int_{A=0}^{A=s_1} \int_{P=0}^{P=1} \int_{x=(A-Ps_2)/2\sin\theta}^{x=(a+(1-P)s_2)/2\sin\theta} \exp(-x^2/2(\sigma^*)^2)(1 - A/s_1)\, dx\, dP\, dA. \quad (10)$$

Multiplication by $1/\sigma^*$ is necessary to account for the concentration of diffraction spots that lie within $\Delta 2\theta$ (Figure 1). The integration makes use of the following relations which are either well known or are given by Geller and Ng (1969) in the forms shown below or by more general expressions from which the requisite integrals can be derived.

$$\mathrm{erf}(x) = \frac{2}{\sqrt{\pi}} \int_{t=0}^{t=x} \exp(-t^2)\, dt, \quad (11)$$

$$\mathrm{erf}(-x) = -\mathrm{erf}(x), \quad (12)$$

$$\int \mathrm{erf}(x)\, dx = x\, \mathrm{erf}(x) + \frac{1}{\sqrt{\pi}} \exp(-x^2), \quad (13)$$

$$\int x\, \mathrm{erf}(x)\, dx = \frac{x^2}{2} \mathrm{erf}(x) + \frac{x}{2\sqrt{\pi}} \exp(-x^2) - \tfrac{1}{4} \mathrm{erf}(x), \quad (14)$$

$$\int x^2 \mathrm{erf}(x)\, dx = \frac{x^3}{3} \mathrm{erf}(x) + \frac{x^2}{3\sqrt{\pi}} \exp(-x^2) + \tfrac{1}{3} \exp(-x^2), \quad (15)$$

$$\int_{t=0}^{t=x} t \exp(-t^2)\, dt = \tfrac{1}{2}(1 - \exp(-x^2)). \quad (16)$$

The integrations are accomplished by substitution and parts, and the proliferation of terms makes the procedure too long and tedius for a description here. After collection of terms and simplification, the solution is

$$\psi = \frac{1}{\sigma^*}\left[\frac{s_1 + s_2}{12 s_1 s_2} \mathrm{erf}\left(\frac{s_1 + s_2}{Q}\right)(2(s_1 + s_2)^2 + 3Q^2) + \frac{s_1 - s_2}{12 s_1 s_2} \mathrm{erf}\left(\frac{s_1 - s_2}{Q}\right)(2(s_1 - s_2)^2 + 3Q^2) - \frac{1}{6s_1} \mathrm{erf}\left(\frac{s_2}{Q}\right)(2s_2^2 + 3Q^2) - \frac{1}{6s_2} \mathrm{erf}\left(\frac{s_1}{Q}\right)(2s_1^2 + 3Q^2) + \frac{Q}{6\sqrt{\pi} s_1 s_2} \exp(-(s_1 + s_2)^2/Q^2) \cdot ((s_1 + s_2)^2 + Q^2) + \frac{Q}{6\sqrt{\pi} s_1 s_2} \exp(-(s_1 - s_2)^2/Q^2) \cdot ((s_1 - s_2)^2 + Q^2) - \frac{Q}{3\sqrt{\pi} s_1 s_2} \exp(-(s_2/Q)^2)(s_2^2 + Q^2) - \frac{Q}{3\sqrt{\pi} s_1 s_2} \exp(-(s_1/Q)^2)(s_1^2 + Q^2) + \frac{Q^3}{3\sqrt{\pi} s_1 s_2}\right], \quad (17)$$

where $Q = 2\sqrt{2}\sigma^* \sin\theta$. The values for s_1, s_2, and σ^* have the units of degrees. The function erf(x) must be evaluated by an accurate method, such as the polynomial approximation given by Abramowitz and Stegun (1970, Formula 7.1.26).

Eq. (17) should be evaluated by digital computer, though any type of mini or micro computer is suitable for very quick results. The equation is easily incorporated into other computer programs that reduce intensities to F values, or model X-ray diffraction patterns. If the results are applied to General Electric (Diano) or older Norelco diffractometers, Eq. (17) can be considerably simplified because, for these instruments, $s_1 = s_2 = 1$.

Eq. (17) was checked for errors by comparing many solutions for different values of θ, s_1, s_2, and σ^* with the results obtained by computer-calculated numerical integrations of Eq. (10). In all comparisons agreement was better than 0.1%, and that difference is easily accounted for by the finite values that must be assumed for dx, dA, and dP by the numerical method. In short, Eq. (17) is an accurate representation of Eq. (10), and the details of the derivation of the latter have been given here for the reader's scrutiny.

A simplified version of Eq. (10) was developed largely on intuitive grounds. The integration over the powder arc for $P = 0$ is retained (Eq. (5)), and the soller slits are treated as a mean square composite,

$$\bar{s} = \sqrt{s_1^2 + s_2^2}. \quad (18)$$

The correction for beam flux (Eq. (9)) is set equal to

$$1 - 2 \sin\theta x/\bar{s},$$

and the final form is

$$\psi \propto \int_{x=0}^{x=a=\bar{s}/2\sin\theta} \exp(-x^2/2(\sigma^*)^2) \cdot(1 - 2\sin\theta x/\bar{s})\, dx. \quad (19)$$

The beam flux correction diminishes the X-ray intensity with respect to x so that the flux equals zero at the limit of the integration.

Integration is accomplished by parts and by substitution. For the first step, Eq. (19) is expressed by two parts, namely

$$\int_{x=0}^{x=\bar{s}/2\sin\theta} \exp(-x^2/2(\sigma^*)^2)\, dx, \quad (20)$$

and

$$\frac{-2\sin\theta}{\bar{s}} \int_{x=0}^{x=\bar{s}/2\sin\theta} x \exp(-x^2/2(\sigma^*)^2)\, dx. \quad (21)$$

Eq. (20) is integrated by making use of Eq. (11) and by the substitution,

$$t = x/\sqrt{2}\sigma^*, \quad \text{or} \quad x = \sqrt{2}t\sigma^*.$$

Then,

$$\sqrt{2}\sigma^* \int_{t=0}^{t=\bar{s}/2\sqrt{2}\sin\theta\sigma^*} \exp(-t^2)\, dt = \frac{\sqrt{2\pi}\sigma^*}{2} \operatorname{erf}(\bar{s}/2\sqrt{2}\sin\theta\sigma^*). \quad (22)$$

The solution of Eq. (21) makes use of Eq. (16) and the same substitutions, so

$$-\left(\frac{2\sin}{\bar{s}}\right)(\sqrt{2}\sigma^*)^2 \int_{t=0}^{t=\bar{s}/2\sqrt{2}\sin\theta\sigma^*} t\exp(-t^2)\, dt = -\frac{2\sin\theta(\sigma^*)^2}{\bar{s}}(1 - \exp(-(\bar{s}/2\sqrt{2}\sin\theta\sigma^*)^2)). \quad (23)$$

Multiplying by $s_1 s_2/\bar{s}(\sigma^*)^2$ makes the absolute values properly dependent on σ^* and s_1 and s_2, and when Q is substituted for $\bar{s}/2\sqrt{2}\sin\theta\sigma^*$, the final result is

$$\psi = \frac{s_1 s_2}{\bar{s}(\sigma^*)^2}\left[\frac{\sqrt{2\pi}\sigma^*}{2}\operatorname{erf}(Q) - \frac{2\sin\theta(\sigma^*)^2}{\bar{s}}(1 - \exp(-Q^2))\right]. \quad (24)$$

The derivation of Eqs. (17) and (24) involves the simplification of substituting the argument for the arcsine of the argument that defines the upper integration limit of the first integral. In addition, the simplified form of Eq. (24) is an approximation. To test the overall errors involved, calculations were made for ψ by a numerical, computer procedure that utilized a form of Eq. (10) that included the correct arcsine variable. These were compared with solutions of Eq. (24). Results are based on two values of soller slit collimation, 3.3° and 1°, and 1° and 1°, and for values of σ^* of 4°, 10°, 20°, and 30°. The range of conditions covers two different

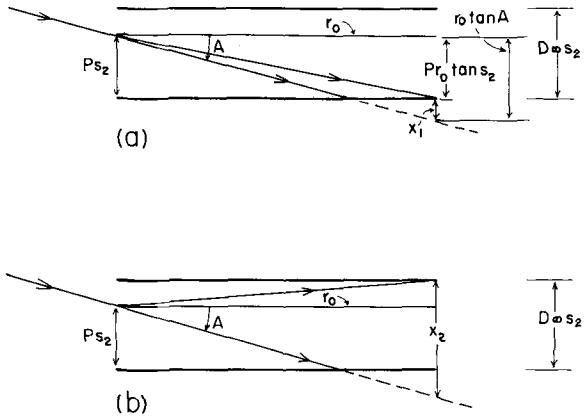

Figure 2. Diffraction geometry leading to the limits of integration (x_1, x_2) of text Eq. (10). A is angle of incident radiation; s_2 is the divergence of the diffracted beam soller slit; r_0 is the goniometer radius; P is the position of a diffracting increment of powder, expressed as a decimal fraction of the spacing of the plates in the diffracted beam soller slit.

and currently used diffraction optics, and the range of preferred orientations likely to be encountered in oriented clay aggregates. The agreement between the two methods for computation of ψ was evaluated between 3° and 80°2θ. For all comparisons save one, all differences are less than 3%. The one exception is the most extreme case, $s_1 = 3.3$, $s_2 = 1$, and $\sigma^* = 30°$, for which errors of 4 to 5% occur below 5°2θ.

The comparison demonstrates that the simplified and approximate form of Eq. (24) is adequate for most work that utilizes X-ray diffraction intensities, and that the use of the cumbersome expression of Eq. (17) is unwarranted. Eq. (17) is included here, however, because it is entirely justifiable on simple geometric grounds, whereas Eq. (24) is not.

EXPERIMENTAL

Diffraction patterns

Chlorite from the Silurian Bertie Formation of northeastern New York State was used to test the theory developed above. The limestone was crushed and treated with HCl to remove carbonate, and the insoluble residue was washed to dispersion with water. The <1-μm e.s.d. fraction was recovered by centrifuge and treated with Chlorox to remove organic material. X-ray powder diffraction studies of the clay show it to consist of a high-magnesium chlorite mixed with illite. Comparisons between air-dried and ethylene glycol-solvated preparations disclosed that the chlorite is slightly expandable, based on changes of peak height and shape after glycolation.

X-ray powder diffraction mounts were prepared by three different methods: (1) centrifugation onto an unglazed ceramic tile, (2) vacuum filtration through a tile, and (3) vacuum filtration through a Millipore GA-6

Table 1. Intensity data for chlorite from the Bertie Formation, New York State.

Reflection	$s_1 = 1°; s_2 = 1°$ Raw data (count/sec)	$s_1 = 1°; s_2 = 1°$ Corr. data[1] (count/sec)	$s_1 = 3.3°; s_2 = 1°$ Raw data (count/sec)	$s_1 = 3.3°; s_2 = 1°$ Corr. data[1] (count/sec)
$\sigma^* = 4.3$ (centrifuged onto a porous plate)				
001	5037	970	11,020	1037
002	4837	716	13,820	787
004	4588	613	17,030	668
005	997	131	4007	146
$\sigma^* = 6.1$ (suction Millipore filter-glass transfer)				
001	3654	1162	7920	1113
002	3452	953	9780	892
004	3067	807	11,080	784
005	680	177	2490	169
$\sigma^* = 12.8$ (suction through a porous plate)				
001	861	969	2277	834
002	674	765	2291	693
004	561	640	2105	596
005	126	143	471	132

[1] Corrected values refer to $s_1 = s_2 = 1°$, and $\sigma^* = 12°$.

0.45-μm filter, followed by inversion of the clay film onto a glass slide. The preparations were thick enough (~20 mg/cm^2) to eliminate the effects of the surface texture of the tiles, and, in conjunction with the relatively high mass absorption coefficient ($\bar{\mu}^* \sim 45$), to ensure infinite thickness for X-ray diffraction at the maximum angles recorded. Ethylene glycol solvation was accomplished by exposure to the vapor at 60°C for 24 hr.

X-ray diffraction measurements were made with an automated Siemens D-500 diffractometer equipped with a copper tube and a graphite monochromator. Tube settings were 40 kV and 30 mA. All intensities are integrated values obtained with step-scanning procedures, corrected for the effects of an interpolated linear background. One-degree divergence slits were used for the range above 12°2Θ, and 0.3° slits were employed at smaller angles to ensure that the spread of the incident beam defined an area smaller than the sample surface. The low-angle intensities were normalized to that of the 002 reflection. Data were obtained with two different soller slit arrangements. One set was measured with the standard Siemens geometry which consists of a one-degree diffracted beam slit, and no incident beam slit. The other was measured with one-degree soller slits in both positions.

The accuracy of the intensities depends on the peak to background ratio and on the number of counts recorded during peak integration. The count total was adjusted for each of the peaks in each run so that the standard deviation is <2% (Klug and Alexander, 1974, p. 362). The estimated standard deviation is 3.3% for the chlorite 005 reflection from the sample prepared by vacuum filtration onto a ceramic tile, measured with both soller slits in place. The intensity data are shown in Table 1.

Eleven specimens of illite or highly illitic illite/smectite, <1- or <0.5-μm e.s.d., were prepared as suspensions and were centrifuged onto porous ceramic tiles and solvated with ethylene glycol, and the integrated intensity was measured for the illite 003 (or illite 003/smectite 005) reflection. A one-degree divergence slit was employed with the primary beam soller slit not in place. The results are shown in Table 2. During the period of data collection, the instrument gave a peak intensity of 18,700 count/sec for the quartz reflection, at 26.65°2θ, from a Diano Permaquartz standard.

The standard Siemens D-500 diffractometer was not equipped with a primary beam soller slit, so the effective axial divergence of the incident beam was measured. If σ^* and 2θ are large, intensity is proportional to $s_1 s_2$. Integrated peak areas for the quartz reflection at ~26.6° were obtained with and without a one-degree primary beam soller slit that is available from Siemens. The ratio of the quartz intensities without/with s_1 in

Table 2. Integrated intensities in count/sec for the reflection near 26.6°2θ from illite and illite/(glycolated) smectite.

Formation	Locality, age	% Expandable	σ^*	Raw data I(003)	Corrected to $\sigma^* = 12°$ I(003)
Duvernay	Alberta, Devonian	~0	6.03	15,020	3860
Silver Hill	Montana, Cambrian	0	8.09	7500	3430
Kalkberg	New York, Devonian	10	6.02	17,180	4420
Sylvan	Oklahoma, Ordovician	~5	8.40	7840	3860
Gunflint	Minnesota, Precambrian	10	6.90	12,520	4180
Onondaga	New York State, Devonian	10	5.94	16,080	4000
Madison	Wyoming, Mississippian	0	4.45	27,790	3950
Mancos	New Mexico, Cretaceous	10	12.5	3540	3820
Interlake	Montana, Silurian	0	5.90	13,840	3400
Salona	Pennsylvania, Ordovician	10	5.31	19,340	3870
Gros Ventre	Wyoming, Cambrian	~5	6.59	13,580	4140
			Mean	14,020	3900
			Standard deviations	±46.6%	±7.7%

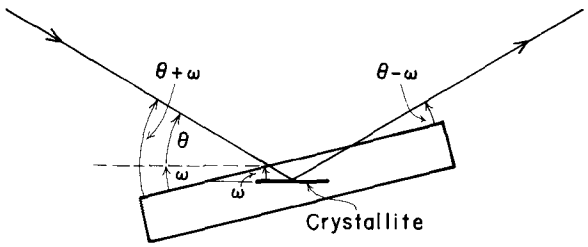

Figure 3. Diffraction geometry for measurement of preferred orientation. ω is the tilt angle of the sample from the normal θ/2θ condition.

place was 4.07. The primary slit (s_1) had a clear area of 81%, that is, 19% was obstructed by the edges of the 24 plates in the assembly. So the effective value of s_1 with the one-degree slit absent was

$$4.07 \times 0.81 = 3.3°.$$

Corrections for intensities obtained with or without s_1 in place required the use of 1° and 1° or 1° and 3.3° in Eq. (24), with the additional step of dividing by 0.81 the results obtained with the one-degree slit. Corrections for slit area (81%) were required only if absolute intensities were to be compared for the two soller-slit configurations.

Preferred orientation

The D-500 diffractometer provides separate control of the incident angle θ by means of a computer-controlled stepping motor. This arrangement makes possible the measurement of the orientation function by means of procedures used in preparing a one-dimensional pole figure. Figure 3 shows a schematic of the geometry. The horizontal dashed line represents the sample surface for the normal mode of diffractometry. The powder sample has been tilted by the angle ω, thus bringing into the reflection condition a crystallite in the powder whose basal plane makes the angle ω with respect to the powder surface. The standard deviation of the orientation function was measured by obtaining intensities from a single reflection for the successive values of ω. For these measurements, the incident beam soller slit and the diffracted beam scatter slit were removed from the diffractometer. The intensities were integrated because the diffractometer focus deteriorated as ω departed more and more from zero. In addition, a correction was applied to account for the asymmetrical path lengths of the incident and diffracted beams, and for the change in area illuminated as a function of ω. The correction consisted of multiplying the measured intensities by (James, 1965, p. 334)

$$1 + \frac{\sin(\theta + \omega)}{\sin(\theta - \omega)}, \qquad (25)$$

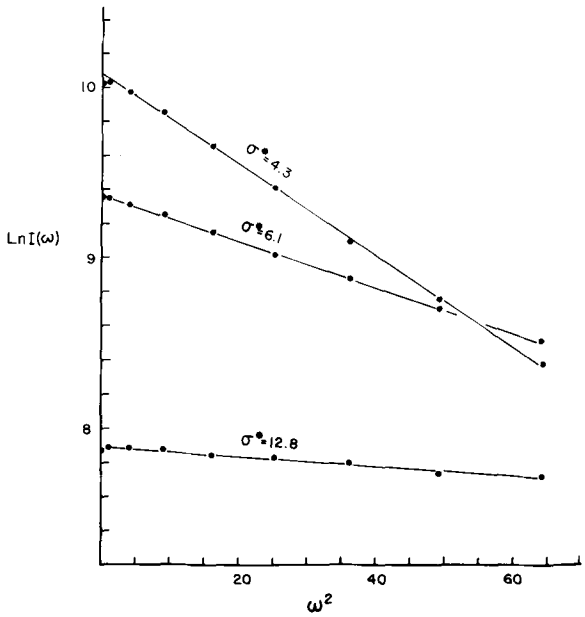

Figure 4. Plot of intensity as a function of tilt angle (I(ω)) vs. ω^2. σ* is the standard deviation of the orientation function, and is given by the reciprocal of two times the slope. Data refer to the Bertie chlorite.

where θ is the Bragg angle, in this case, the position of the chlorite 004 reflection or 12.5°.

Suppose an array (I(ω)) of corrected, integrated intensities at different values of ω. Intensity is proportional to the number of crystallites, N(ω), that are oriented in such a way as to diffract into the detector aperture. If the orientation function is Gaussian,

$$I(\omega) \propto N(\omega) = k \exp(-\omega^2/2(\sigma^*)^2), \qquad (26)$$

where k is a constant. Taking the logarithms of both sides yields

$$\ln(I(\omega)) = -\frac{\omega^2}{2(\sigma^*)^2} + \ln k. \qquad (27)$$

A plot of I(ω) vs. ω^2 gives a straight line whose slope is $\frac{1}{2}(\sigma^*)^2$ and whose intercept is ln k. The slope easily yields σ*, the standard deviation of the orientation function.

Figure 4 shows such plots for the three samples described here. The excellent fit of the data to straight lines verifies that the orientation function was indeed Gaussian. These findings are in agreement with those of Taylor and Norrish (1966), Lippmann (1970), and Hall *et al.* (1983) who, using different experimental arrangements, concluded that a Gaussian function adequately explains the orientation state of well-oriented clays. The present writer has made more than 100 determinations on other clay samples, and, based on

Table 3. Intensity data for chlorite from the Bertie Formation, New York State. All values are normalized to a constant intensity for the chlorite 005 reflection.

Reflection	$s_1 = 1°; s_2 = 1°$		$s_1 = 3.3°; s_2 = 1°$	
	Raw data (count/sec)	Corr. data[1] (count/sec)	Raw data (count/sec)	Corr. data[1] (count/sec)
		$\sigma^* = 4.3$		
001	758	1111	413	1065
002	728	820	517	809
004	690	702	638	721
005	150	150	150	150
		$\sigma^* = 6.1$		
001	806	985	477	988
002	761	808	589	792
004	677	684	667	696
005	150	150	150	150
		$\sigma^* = 12.8$		
001	1025	1016	725	948
002	802	802	730	788
004	668	671	670	677
005	150	150	150	150

[1] Corrected values refer to $s_1 = s_2 = 1°$, and $\sigma^* = 12°$.

this experience, the impressive fit shown by Figure 4 is by no means exceptional. Note that for the first few points $\omega = 0$ and $\omega = 1$, the data fall off of the lines and, indeed, have been disregarded in fitting the lines. In the writer's experience, this phenomenon is always present and its cause is unknown. It was exacerbated if the diffracted beam scatter slit was left in place.

Values of σ^* obtained by these procedures for the three preparations of the Bertie chlorite and the eleven illite samples are listed in Tables 1–3.

DISCUSSION

Table 1 shows the raw intensity data for the Bertie chlorite and corrected versions of the same. The intensities measured with the primary soller slit absent were diminished by 19% to compensate for the area of s_1 obscured by the plate assembly. Then all intensities were corrected by means of Eq. (24). For each set, the appropriate value of ψ was removed by division, and the data set was then multiplied by ψ for $\sigma^* = 12$ and $s_1 = s_2 = 1°$.

Inspection of the raw data in Table 1 shows the very large variation in intensity caused by the soller slit configurations and by variations in σ^*. The corrections went a long way toward eliminating these differences, though the corrected data still retained significant variability. The Bertie sample studied here was not an ideal one to demonstrate that the theory accounts for absolute intensity variations, inasmuch as the material is a mixture of chlorite and illite, and particle size separations during sample preparation could have introduced other variables in the intensity data. Still, a very large portion of the scatter has been eliminated by the application of Eq. (24).

A more appropriate test of the validity of absolute intensities was provided by the results for illite (Table 2). The column labelled I(003) shows a wide range in intensity values, approximately a factor of eight; however, when corrected to the common base of $\sigma^* = 12$ by Eq. (24), the standard deviation about the mean amounted to only ±7.7%. No account was taken of possible variations in $\bar{\mu}^*$ or of the effects of Fe or K substitutions that differ from nominal values. The results indicate that absolute intensities were controlled primarily by preferred orientation, and that the theory described here is adequate to account for differences in illite peak intensities from sample to sample.

The primary goal of this work was to evaluate the angle-dependent character of ψ or of the Lorentz factor. Table 3 shows raw and corrected data that have been normalized to a constant integrated intensity for the 005 reflection. The low diffraction angles were most sensitive to variations in soller slit divergence and in σ^*, and the raw data show that a factor of 2.5 was present in the extreme cases for the intensity of the 001. Inspection of the raw data reveals the kinds of errors that can be involved if different instruments and different methods of sample preparation are utilized.

The corrected data sets were very similar to one another. The worst case discrepancy was a factor of 1.17 for the 001, and the standard deviation of the six 001 intensities about the mean amounted to ±5.8%. This value is probably very close to the precision which is realized by routine measurements of low-angle diffraction intensities, for these are sensitive to sample smoothness, flatness, and small errors in the 2:1 alignment of the sample.

The agreement between theory and experiment implies the fundamental correctness of Eq. (24). Further refinements could have been made by incorporating the effects of other geometrical factors, but any improvement is likely to be of the same order as the precision with which intensities were measured from sample to sample. At the present time, such additions to the theory seem unwarranted.

PRACTICAL APPLICATIONS

The random-powder Lorentz factor appears to be a good approximation for samples with poor ($\sigma^* > 15$) degrees of preferred orientation that are analyzed by means of instruments that incroporate 2 one-degree (factory designation, two-degree) soller slits. This example provides an error of 10% at $5°2\theta$, and, of course, much smaller errors at high values of 2θ. If orientation is good, as evidenced by unusually high recorded intensities, simply solving Eq. (24) for $\sigma^* = 12$ is likely to provide satisfactory values for ψ. In the writer's experience, the centrifuged porous plate method produces very high preferred orientations ($\sigma^* = 5$ to 10), and this method should be avoided unless σ^* is measured.

Such simple solutions are not feasible if the diffraction geometry contains only one soller slit. The Lorentz factor then is much more dependent on σ^* within the range of values commonly encountered for that variable. The poorest choice, but one that is better than either the single crystal or random powder options, is simply to assume that $\sigma^* = 12$, and correct the data accordingly.

Another option used in the writer's laboratory produces estimates of σ^* that are useful for correcting relative intensities on a given diffractogram. Repeated solutions of Eq. (24) show that, to a very good approximation, the intensity of a reflection at moderate values of 2θ ($\sim 25°$) is proportional to $1/(\sigma^*)^2$. This relation suggests that, with proper instrumental calibration, the absolute intensity of, e.g., the illite 003 reflection, in a pure monomineralic aggregate is a sensitive measure of σ^* (see Table 2).

Let QI be the quartz reference intensity (peak height in count/sec at 26.64°2θ, "permaquartz" standard), I(003) the integrated intensity of the illite 003 reflection, and $\bar{\mu}^*$ the mass absorption coefficient of the sample (CuKα radiation), and assume a nominal value of 45 for the mass absorption coefficient of illite. Then,

$$\sigma^* = \sqrt{\frac{KQI}{I(003)} \cdot \frac{45}{\bar{\mu}^*}}, \qquad (28)$$

where K is a constant which can be evaluated from the data in Table 2, *viz.*

$$12 = \sqrt{\frac{K18{,}700}{3903} \cdot \frac{45}{45}}; \quad K = 30.1.$$

The utility of Eq. (28) can be extended by making use of mineral intensity factors for other clays. Reynolds (1980) showed that, at constant $\bar{\mu}^*$, the integrated intensities of the (glycolated) smectite 005, the illite 003, and the interstratified illite/(glycolated) smectite 003/005 reflections are very similar. The kaolinite 002 reflection is about twice as intense as the chlorite 004 reflection for types of chlorite commonly found in sedimentary rocks. Consequently, I(003) in Eq. (28) can be replaced with I(26.6) + I(25)/2, where the quantities in parentheses refer to 2θ values, and

$$\sigma^* = \sqrt{\frac{30.1QI}{I(26.6) + I(25)/2} \cdot \frac{45}{\bar{\mu}^*}}. \qquad (29)$$

Such a procedure gives values of σ^* that are unaffected by soller slit configurations, divergence slit selection, tube operating conditions, etc., because these variables are compensated for by changes in the quartz reference intensity (QI). The method will work for clay aggregates composed essentially of illite, smectite, interstratified illite/smectite, kaolinite, and chlorite. If quartz is present, its contribution to the ~26.6° reflections must be eliminated by making use of the quartz peak at 20.8°2θ. The procedure may seem too full of approximations and/or unknown quantities to be of much use, but it succeeds because the square-root dependence means that errors in the quotients do not seriously affect σ^*.

CONCLUSIONS

(1) The geometrical components of angle-dependent and absolute intensity variations can be described by a closed-form equation that depends on soller-slit collimation and the degree of preferred orientation in oriented clay aggregates.

(2) Clay mineral specimens belonging to the same species give very similar diffraction intensities. Inter- and intralaboratory differences are caused by variable instrumental parameters and, most importantly, by differences in preferred orientation which is controlled by sample preparation procedures and by crystallite morphology. For chlorites, variations in chemical composition may cause large changes in peak intensities that are independent of instrument or orientation factors.

(3) The preferred orientation of clays produced by evaporation, centrifugation, or suction methods follows an axially symmetrical Gaussian function.

(4) Preferred orientation produced by the above methods can be completely described by a single parameter, σ^*.

(5) σ^* can be measured by means of a one-dimensional pole figure determination, or it can be approximated by consideration of absolute diffraction intensity.

ACKNOWLEDGMENTS

The author is grateful for space and facilities provided by the University of Illinois during a sabbatical leave. Some of the concepts described above were developed at that time. In addition, support is acknowledged by the National Science Foundation under Grants EAR-75-21836 and EAR-82-06188.

REFERENCES

Abramowitz, M. and Stegun, A. (1970) *Handbook of Mathematical Functions:* Dover, New York, 1046 pp.

Geller, M. and Ng, E. W. (1969) A table of integrals of the exponential integral: *J. Res. Nat. Bur. Stds.—B. Math. and Math. Sci.* **738,** 191–210.

Hall, P. L., Harrison, R., Hayes, M. H. B., and Tuck, J. J. (1983) Particle orientation distributions and stacking arrangements in size-fractionated montmortillonite measured by neutron and X-ray diffraction: *J. Chem. Soc. Faraday Trans.* **79,** 1687–1700.

James, R. W. (1965) *The Optical Principles of the Diffraction of X-Rays:* Cornell Univ. Press, Ithaca, New York, 664 pp.

Klug, H. P. and Alexander, L. E. (1974) *X-Ray Diffraction Procedures:* Wiley, New York, 966 pp.

Lippmann, F. (1970) Functions describing preferred orientation in flat aggregates of flake-like clay minerals and in

other axially symmetric fabrics: *Contr. Mineral. Petrol.* **25,** 77–94.

MacEwan, D. M. C. (1956) Fourier transform methods for studying scattering from lamellar systems. I. A direct method for analyzing interstratified mixtures: *Kolloid Z.* **149,** 96–108.

Reynolds, R. C. (1976) The Lorentz factor for basal reflections from micaceous minerals in oriented powder aggregates: *Amer. Mineral.* **61,** 484–491.

Reynolds, R. C. (1980) Quantitative analysis of kaolinite, illite, and mixed-layered illite-smectite by X-ray diffraction methods: in *Prog. Abstracts, 29th Ann. Clay Conf., Urbana, Illinois,* p. 83.

Taylor, R. M. and Norrish, K. (1966) The measurement of orientation distribution and its application to quantitative X-ray diffraction analysis: *Clay Miner.* **6,** 127–142.

(Received 6 April 1984; accepted 11 November 1984; Ms. 1351)